Contents lists available at SciVerse ScienceDirect

Solar Energy Materials & Solar Cells

journal homepage: www.elsevier.com/locate/solmat

Degradation of photovoltaic devices at high concentration by space charge limited currents

CrossMark

Ari Feldman [a,b,*], Richard Ahrenkiel [a,c], John Lehman [b]

[a] Colorado School of Mines, Golden, CO, United States
[b] National Institute of Standards and Technology, Boulder, CO, United States
[c] National Renewable Energy Laboratory, Golden, CO, United States

ABSTRACT

High-injection mobility reduction is examined by theory, modeling, and experimental data acquired by resonance-coupled photoconductive decay (RCPCD). The ambipolar mobility is shown to reduce to zero when the constituent injection-dependent carrier mobilities are taken into account. Modeling of the photoconductivity incorporating the transient, injection-dependent, ambipolar mobility confirms experimental reduction in signal at increasing carrier-generation rates. The onset of the reduction of mobility occurs at approximately 10 times the background carrier density; thus devices that utilize lightly doped materials are susceptible to anomalous injection-based behavior. For photovoltaic applications, high-injection device-performance degradation would result from mobility reduction due to reduced diffusion length.

© 2013 Elsevier B.V. All rights reserved.

With the increasing popularity of concentrated photovoltaics (PV), the behavior of the PV material at high optical injection level is critical. One of the key issues in silicon-based devices is the dominance of Auger recombination at high injection levels. An additional issue that we address in this work is a decrease in the mobility of all PV materials because of space-charge effects. Here we have measured the ambipolar mobility at high injection by combining transient photoconductive decay (PCD) and transient free-carrier absorption (FCA) at identical injection levels. As the PCD signal is proportional to $\Delta n \mu$ and the FCA varies as $\Delta n/\mu$, the mobility can be extracted from the ratio of the measurements.

Prior work has shown high-injection behavior including surface recombination velocities [1–4] and minority-carrier lifetimes [5] that influence solar-cell performance. With the increasing popularity of concentrator technology, high-injection effects must be considered during both device design and characterization. Rein [6] and others [2] have investigated injection-dependent lifetime phenomena where increasing intensities led to increased bulk lifetime. There are many factors that can reduce carrier lifetime at high injection, including Auger recombination [7] and carrier–carrier scattering [8], while an important factor for traditional semiconductors and organic solar cells, high-injection mobility reduction has largely been overlooked as an aspect of conventional photovoltaic device physics.

When an optical excitation produces excess electrons and holes, the resulting excess carrier behavior is controlled by the recombination processes (band-to-band, Shockley–Read–Hall, Surface, and Auger) [9]. The transient excess carrier concentration and recombination processes can be accurately described by the photoconductive decay. Photoconductive measurements measure the minority-carrier lifetime from the slope of the transient decay, which depends on the recombination behavior of the excess carriers. The various recombination processes have a wide range of time constants that can be extracted at different points along the waveform. A single exponential decay is typical for bulk materials at low-injection. Photoconductive decay can be described in the equation

$$\Delta\sigma(t) = q(\Delta n(t)\mu_n + \Delta p(t)\mu_p), \tag{1}$$

where $\Delta\sigma(t)$ is the transient photoconductivity, q is the fundamental charge of an electron, $\Delta n(t)$ and $\Delta p(t)$ are the transient excess carrier concentrations of electrons and holes, and μ_n and μ_p are the electron and hole mobilities, respectively. Currently, for all photoconductive decay measurements, the electron and hole mobilities are often assumed constant or invariant with time and injection through all excitation ranges.

This approximation works for low-injection conditions when the excess free-carrier concentration is much less than the background-carrier concentration of the sample. In the low-injection regime, the minority-carrier capture controls the lifetime. At higher injection however, the recombination becomes a complex function of the injection level, and electron and hole capture cross section.

The derivation of the ambipolar mobility may be found in many semiconductor textbooks but most notably by Smith [10]. The

* Corresponding author at: National Institute of Standards and Technology, Boulder, CO, United States. Tel.: +1 3034974969.
E-mail address: ari.feldman@nist.gov (A. Feldman).

derivation accounts for high-injection effects when the excess carrier concentration exceeds the dopant concentration. The ambipolar transport equation is composed of the recombination, diffusion, and drift of carriers. Combining the drift-diffusion equations with Poisson's equation, one gets

$$\frac{\partial \Delta p}{\partial t} = -\frac{\Delta p}{\tau_p} + D_a \frac{\partial^2 \Delta p}{\partial x^2} - \mu_a E \frac{\partial \Delta p}{\partial x}, \tag{2}$$

where τ_p is the carrier lifetime, D_a is the ambipolar diffusion coefficient, μ_a is the ambipolar mobility, and E is the electric field. The ambipolar diffusion coefficient is a function of the specific conductivity (σ_n and σ_p) and diffusion coefficient (D_n and D_p) of each carrier:

$$D_a = \frac{\sigma_n D_p + \sigma_p D_n}{\sigma_n + \sigma_p} = \frac{n\mu_n D_p + p\mu_p D_n}{n\mu_n + p\mu_p}. \tag{3}$$

By use of the Einstein relation ($D = \mu kT/q$), this can be reduced to

$$D_a = \frac{n + p}{\frac{n}{D_p} + \frac{p}{D_n}}. \tag{4}$$

Additionally, we can solve for the ambipolar mobility and apply the Einstein relation for simplification as well

$$\mu_a = \frac{\sigma_n \mu_p - \sigma_p \mu_n}{\sigma_n + \sigma_p} = \frac{n - p}{\frac{n}{\mu_p} + \frac{p}{\mu_n}} = \frac{p_0}{\frac{n}{\mu_p} + \frac{p}{\mu_n}} \tag{5}$$

It is obvious to see from Eq. (5) that the ambipolar mobility approaches 0 as the ratio of the background carrier density to the total carrier concentration decreases with higher injection levels. Returning to the ambipolar transport equation in Eq. (2), for continuity to occur, when the mobility approaches zero, the electric field must increase in magnitude. This can be explained by the increased density of free-carriers which creates a space charge plasma, where the internal electric field of the optically generated electron–hole plasma exceeds the built-in electric field of the dopant concentration. Therefore, within the plasma region the mobility is reduced until recombination reduces the carrier density.

While this derivation accounts for high-injection conditions when n approaches p, it fails to account for the carrier-dependent mobility with respect to time. Additionally, we must consider the total carrier concentration, including the background carrier density and the optically generated excess carriers, as the dopant concentration provides a lower limit for conductivity. The total carrier concentration n is composed of the transient excess carrier concentration $\Delta n(t, \Delta n_0)$ and the background carrier density n_0:

$$n(t, \Delta n_0) = \Delta n(t, \Delta n_0) + n_0 \tag{6}$$

$$\Delta n(t, \Delta n_0) = \Delta n_0 e^{-t/\tau} \tag{7}$$

$$\Delta n_0 = \alpha I_0 e^{-\alpha x} \tag{8}$$

The excess carrier concentration is further defined by the volume generation Δn_0 and the carrier lifetime τ. The volume generation is composed of the incident energy I_0, the absorption coefficient α, and the thickness of the sample x. Similar equations may also be derived for holes, where $\Delta n(t, \Delta n_0) = \Delta p(t, \Delta p_0)$.

Mobility as a function of the dopant concentration has also been previously derived [11,12] with respect to carrier–carrier scattering and here we expand that model to include the total transient carrier concentration:

$n-type\ Si$

$$\mu_n(t, \Delta n_0) = 65 + \frac{1265}{1 + \left(\frac{n(t, \Delta n_0)}{8.5 \times 10^{16}}\right)^{0.72}}$$

$$\mu_p(t, \Delta n_0) = 130 + \frac{370}{1 + \left(\frac{p(t, \Delta n_0)}{8 \times 10^{17}}\right)^{1.25}} \tag{9}$$

$p-type\ Si$

$$\mu_n(t, \Delta n_0) = 232 + \frac{1180}{1 + \left(\frac{n(t, \Delta n_0)}{8 \times 10^{16}}\right)^{0.9}}$$

$$\mu_p(t, \Delta n_0) = 48 + \frac{447}{1 + \left(\frac{n(t, \Delta n_0)}{6.3 \times 10^{16}}\right)^{0.76}}. \tag{10}$$

Finally, we may insert the transient-carrier concentration-dependent mobility and transient total-carrier concentrations back into Eq. (5), garnering a transient, injection-dependent, ambipolar mobility:

$$\mu_a(t, \Delta n_0) = \frac{n(t, \Delta n_0) - p(t, \Delta n_0)}{\frac{n(t, \Delta n_0)}{\mu_p(t, \Delta n_0)} + \frac{p(t, \Delta n_0)}{\mu_n(t, \Delta n_0)}}. \tag{11}$$

Furthermore, using this new ambipolar mobility in the photoconductive decay equation, which accounts for total carrier concentration, allows for the demonstration of the injection dependence with respect to time,

$$\Delta\sigma(t, \Delta n_0) = q\mu_a(t, \Delta n_0)(n(t, \Delta n_0) + p(t, \Delta n_0)). \tag{12}$$

Photoconductivity data were acquired by the use of the resonance-coupled photoconductive decay [13] (RCPCD) technique on an unpassivated p-type (100) Si wafer. The RCPCD apparatus can be seen in Fig. 1a and is composed of an RF coil operating at approximately 500 MHz that magnetically induces eddy currents in the free-carriers of an illuminated sample. The photoconductive signal is acquired by measuring the transient impedance difference between the input coil signal and the mutual impedance of the sample. The impedance difference between the coil alone and an illuminated sample can be seen in Fig. 1b. The circuit operates at 50 Ω, so the frequency and phase are tuned at low intensity so that the phase component is nullified. This tuning allows the user to tune the signal so that there is a balance of maximum amplitude and best fits a single exponential decay. The exact details of RCPCD operation may be found elsewhere [14].

While this mobility reduction was seen experimentally in many Si substrates of varying doping concentration and polarity, this correlation of theory and results will focus on a single sample that is typical for solar cells. This p-type (100) silicon wafer is polished on one side, has a thickness of ~350 μm, and the wafer manufacturer listed 10–30 Ω cm resistivity. Capacitance–voltage (CV) measurements [15] were performed on this sample, and the dopant density was found to be 1.55×10^{14} cm^{-3}. The low-injection RCPCD lifetime was measured and determined to be ~5 μs, based on the single exponential time constant.

For high-injection conditions, the RCPCD low-injection phase and frequency settings remained constant and the lamp voltage of the 1064 nm YAG laser was systematically increased. Instantaneous waveform data acquisition and beam-power measurements were taken to ensure accurate injection conditions for each data set. The 3 mm YAG beam was incident on a beam splitter, and the areal flux was measured with a thermopile detector. The beam was further expanded to an area of ~0.9 cm^2, the latter of which was incident on the sample. A combination of the computer-controlled lamp voltage and neutral density filters were used to produce a range of volume generation from $\sim 1 \times 10^{13}$ to 5×10^{16} cm^{-3}. Carrier-volume generation density was then calculated based on the 350 μm sample thickness and the absorption coefficient for silicon at 1064 nm.

The relative conductivity with respect to volume generation ranging from low-injection to high-injection for the p(100) sample can be seen in Fig. 2a. For low carrier densities, a typical single exponential decay is observed. Increasing injection increases the amplitude of the signal until the carrier density approaches the dopant concentration, where a waveform "broadening" occurs. The signal maximum starts to flatten, and there is a shift of the

pulse maximum away from $t=0$ s. For injection higher than the dopant concentration, the $t=0$ s amplitude begins to decrease relative to the maximum and further shifts the maximum peak location away from $t=0$ s. The RCPCD data are acquired by the use of an oscilloscope with AC coupling so that the DC component does not put the signal out of range and so that minute changes can be seen. The background conductivity is masked by the AC coupling, and at very high-injection the signal appears to go negative, when in actuality the conductivity becomes less than the dark conductivity.

Fig. 2b models the photoconductive decay from Eq. (12), which accounts for the transient, injection-dependent, ambipolar mobility. The p(100) material parameters were used for the model, where the incident areal flux is reported in Fig. 2b. Again, for low volume generation (1×10^{13} cm^{-3} and 1×10^{14} cm^{-3}) a typical single exponential decay is demonstrated. At 1×10^{15} carriers/cm^3, when the injection level surpasses the background carrier density, there is a flattening of the exponential decay at the maximum amplitude, and the waveform has "broadened". Further increasing the carrier generation to 1×10^{16} cm^{-3} shows that the mobility has become the dominant variable in the photoconductivity equation, and the $t=0$ s amplitude begins to decrease. Both the 1×10^{17} cm^{-3} and 1×10^{18} cm^{-3} injection conditions further emphasize the effect that the reduction of mobility has on the photoconductive decay. As expected, μ_a and thus $\Delta\sigma$ approach zero at very high-injection, where the density of optically generated excess carriers exceeds the background carrier concentration by three orders of magnitude or more. Fig. 2b demonstrates that the modeled photoconductive behavior at high-injection exhibits the anomalous behavior similar to the experimental conditions. For the 1×10^{18} cm^{-3} injection scenario, the maximum amplitude occurs ~20 μs after the laser pulse has concluded.

The amplitude of the photoconductivity at $t=0$ s also demonstrates the onset of the mobility reduction. Fig. 3 demonstrates the initial amplitude of the experimental data (Fig. 3a) from the p-type (100) silicon sample and the calculated $t=0$ s photoconductivity (Fig. 3b) from Eq. (12), both with respect to injection level. The range of carrier generation is more limited for the experimental data but still exhibits the same style of peak at around approximately 10 times the background carrier density. The experimental photoconductivity peak amplitude occurs at a volume generation of 1.57×10^{15} cm^{-3}, and at 1×10^{15} cm^{-3} for the model based on the material parameters. The slight increase of the $t=0$ s signal for the experimental data at the highest injection occurs because the output amplifiers saturate at a negative voltage of -1 V.
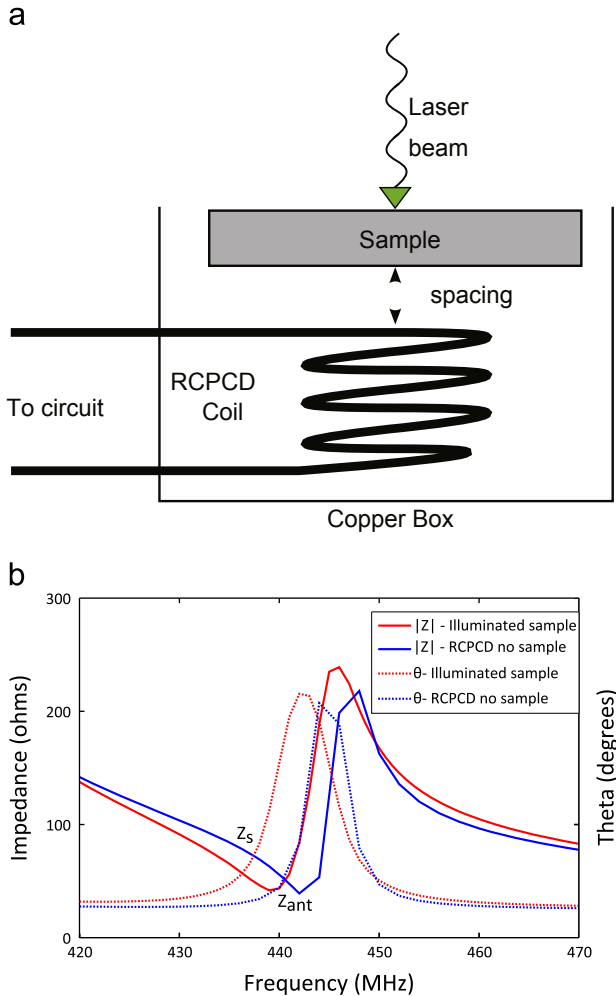

Fig. 1. (a) Resonance-coupled photoconductive decay (RCPCD) schematic. (b) RCPCD impedance and phase tuning points.
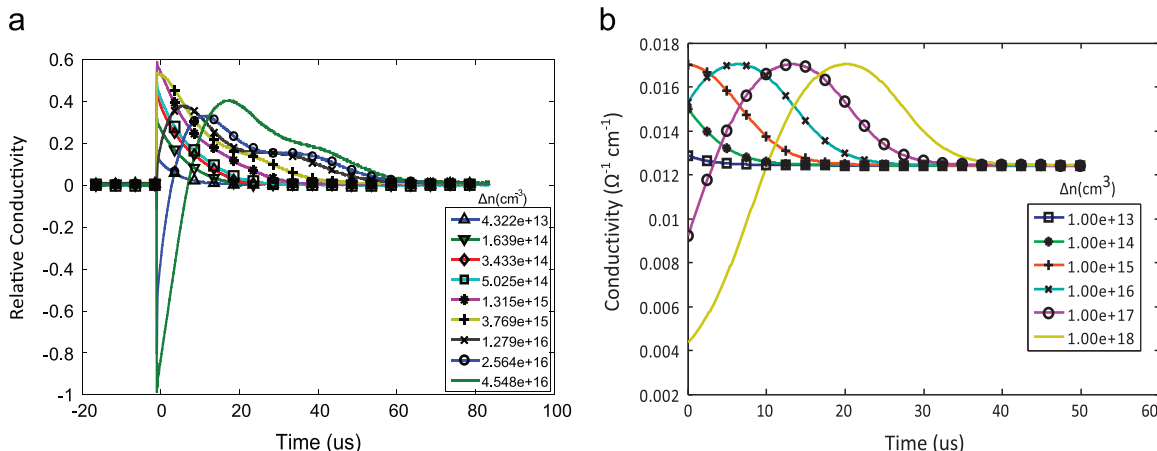

Fig. 2. (a) Photoconductive decay performed on a p(100) silicon wafer with respect to volume generation. (b) Modeled photoconductive decay based on injection-dependent ambipolar mobility calculated from Eq. (11). The $t=0$ "anomaly" is the result of decreased ambipolar mobility at high injection.
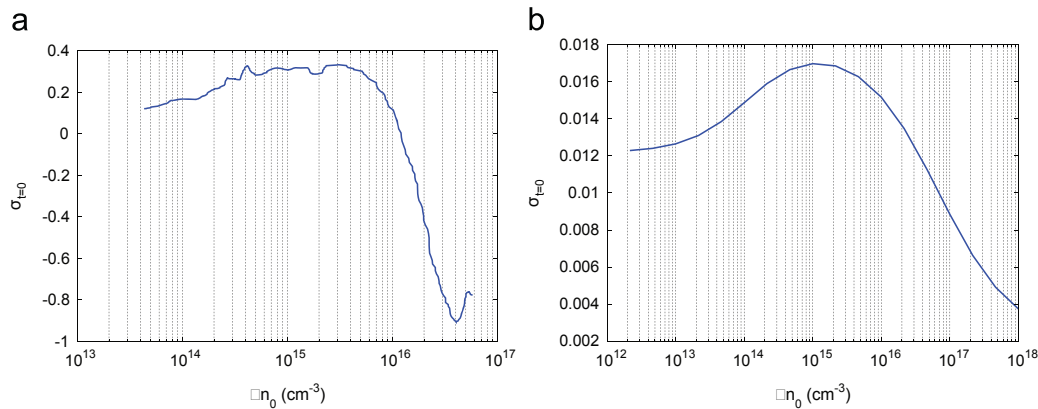
Fig. 3. (a) Data: photoconductive amplitude at $t=0$ s for p(100) silicon wafer as a function of carrier generation. (b) Modeled: $t=0$ s amplitude based on injection-dependent ambipolar mobility by use of the p(100) material parameters.

Qualitatively, the modeled photoconductivity predicts the correct trend, a decrease in initial amplitude and a delay in the peak photoconductive amplitude. The differences between the experimental and the modeled photoconductivities stem from unaccounted variables such as injection-dependent lifetime and additional recombination processes. With regards to the model itself, the empirically derived carrier mobilities from Del Alamo and Caughey were based on ionized donor scattering alone, where here the carrier mobility should account for ionized impurity scattering and carrier–carrier scattering. Also, real-world conditions versus theoretical absorption processes may account for a large variation. The internal quantum efficiency was assumed to be 100% for the calculated volume generation of carriers, where every incident photon creates an electron–hole pair. This also does not account for optical reflections. Therefore, the onset of the mobility reduction may occur closer to the background carrier concentration and not at approximately ten times the background.

It has been shown via theory, modeled data, and experiment that reduction of mobility at high intensities is a significant phenomenon. When the ratio of optically injected carriers exceeds the background carrier density, the ambipolar mobility decreases. The photoconductivity was modeled on actual material parameters and compares well with experimental results. While the data presented here were acquired by the use of RCPCD, similar $t=0$ s behavior was confirmed by the use of a 10 GHz microwave-reflection technique and will be featured in a future publication.

A reduction of mobility at high intensities has severe consequences for photovoltaic device performance as the carriers diffusion length is reduced, thereby affecting device performance. Devices that use lightly doped materials are clearly more susceptible to mobility reduction, as the background carrier density is easily exceeded at concentration. Further examination into the relationship between dopant concentration and mobility reduction will impact predicted device performance.

We have shown the transient excess-carrier decay behavior of crystalline silicon at a range of injection levels. The transient behavior was measured by photoconductive decay techniques and shown that the transient photoconductivity is reduced by an order of magnitude at injection levels corresponding to those found in concentrator solar cells. These effects can be modeled and calculated by using the classic drift-diffusion equations. The results are therefore applicable to most concentrator technology. As such, these findings are a significant factor in concentrator technology.

References

[1] S. Robinson, Recombination saturation effects in silicon solar cells, IEEE Transactions on Electron Devices 41 (1994) 1556–1569.
[2] A.G. Aberle, T. Lauinger, J. Schmidt, R. Hezel, Injection-level dependent surface recombination velocities at the silicon–plasma silicon nitride interface, Applied Physics Letters 66 (1995) 2828–2830.
[3] a.W. Stephens, a.G. Aberle, M.a. Green, Surface recombination velocity measurements at the silicon–silicon dioxide interface by microwave-detected photoconductance decay, Journal of Applied Physics 76 (1994) 363–370.
[4] T. Lauinger, J. Schmidt, Record low surface recombination velocities on 1 Ω cm p-silicon using remote plasma silicon nitride passivation, Applied Physics Letters 68 (1996) 1232–1234.
[5] J. Schmidt, Temperature- and injection-dependent lifetime spectroscopy for the characterization of defect centers in semiconductors, Applied Physics Letters 82 (2003) 2178–2180.
[6] S. Rein, Lifetime Spectroscopy: A Method of Defect Characterization in Silicon for Photovoltaic Applications, Springer Series in Material Science 2005.
[7] J. Schmidt, M. Kerr, P.P. Altermatt, Coulomb-enhanced Auger recombination in crystalline silicon at intermediate and high injection densities, Journal of Applied Physics 88 (2000) 1494.
[8] D. Reznik, W. Gerlach, Injection-level dependence of charge carrier mobility in high-injection plasma, Solid-State Electronics 41 (1997) 405–412.
[9] S. Fonash, Solar Cell Device Physics, 2nd edition, Elsevier, 2010.
[10] R. Smith, Semiconductors, Cambridge University Press, 1961.
[11] D. Caughey, R. Thomas, Carrier mobilities in silicon empirically related to doping and field, Proceedings of the IEEE 55 (1967) 2192–2193.
[12] J. del Alamo, S. Swirhun, R. Swanson, Measuring and modeling minority carrier transport in heavily doped silicon, Solid-State Electronics 28 (1985) 47–54.
[13] R. Ahrenkiel, S. Johnston, An advanced technique for measuring minority-carrier parameters and defect properties of semiconductors, Materials Science and Engineering B 102 (2003) 161–172.
[14] R. Ahrenkiel, Apparatus for Measuring Minority Carrier Lifetimes in Semiconductor Materials, 1999, US Patent 5929652.
[15] M. Li, C. Sah, New techniques of capacitance–voltage measurements of semiconductor junctions, Solid-State Electronics 25 (1982) 95–99.